

Cell Division and Motility Enable Hexatic Order in Biological Tissues


Yiwen Tang^{1,4}, Siyuan Chen², Mark J. Bowick^{2,3}, and Dapeng Bi^{1,4}

¹*Department of Physics, Northeastern University, Boston, Massachusetts 02115, USA*

²*Department of Physics, University of California, Santa Barbara, Santa Barbara, California 93106, USA*

³*Kavli Institute of Theoretical Physics, University of California, Santa Barbara, Santa Barbara, California 93106, USA*

⁴*Center for Theoretical Biological Physics, Northeastern University, Boston, Massachusetts 02115, USA*

 (Received 10 April 2023; accepted 19 April 2024; published 21 May 2024)

Biological tissues transform between solid- and liquidlike states in many fundamental physiological events. Recent experimental observations further suggest that in two-dimensional epithelial tissues these solid-liquid transformations can happen via intermediate states akin to the intermediate hexatic phases observed in equilibrium two-dimensional melting. The hexatic phase is characterized by quasi-long-range (power-law) orientational order but no translational order, thus endowing some structure to an otherwise structureless fluid. While it has been shown that hexatic order in tissue models can be induced by motility and thermal fluctuations, the role of cell division and apoptosis (birth and death) has remained poorly understood, despite its fundamental biological role. Here we study the effect of cell division and apoptosis on global hexatic order within the framework of the self-propelled Voronoi model of tissue. Although cell division naively destroys order and active motility facilitates deformations, we show that their combined action drives a liquid-hexatic-liquid transformation as the motility increases. The hexatic phase is accessed by the delicate balance of dislocation defect generation from cell division and the active binding of disclination-antidisclination pairs from motility. We formulate a mean-field model to elucidate this competition between cell division and motility and the consequent development of hexatic order.

DOI: [10.1103/PhysRevLett.132.218402](https://doi.org/10.1103/PhysRevLett.132.218402)

Organ surfaces are often covered with 2D confluent monolayers of epithelial or endothelial cells, which provide functional separation from the surrounding environment. During development these cells grow, divide, and move, dynamically reorganizing the entire tissue. Regulated by a complex set of chemical and mechanical signaling pathways [1–4], tissue frequently undergoes a transition from a structureless fluidlike state to a state capable of supporting a variety of stresses, most notably elastic stresses [5–11]. Such transformations have recently been analyzed as a crossover from a liquid to an amorphous solid [12,13]. In two-dimensional (2D) systems in equilibrium, however, liquids can develop rigidity via two consecutive transitions, the first corresponding to the development of orientational order without translational order and the second adding translational order to the existing orientational order [14,15]. The intermediate phase with (quasi-long-range) orientational order but translational disorder is known as the hexatic phase and has been shown to occur in a very wide variety of physical systems [16–29]. The hexatic is a particular type of structured fluid since it flows like a fluid but has orientational rigidity.

Previous theoretical and computational models of dense tissues have studied the emergence of hexatic order, with focus on the effects of thermal fluctuations [30–32] and motility [33–36]. Modeling typically studies the inverse process of disordering by melting from the crystalline state.

Realistic tissues, however, are very rarely crystalline with a few exceptions [37,38]. Cell division and apoptosis almost always destroy the crystalline state [39] and yet there has been no direct observation of the hexatic phase in *in vitro* biological tissues, including those undergoing a solid-liquid transition [5,6,8,40]. Recent studies have observed pronounced orientational order associated with cell division during the development of *Drosophila* embryos [41,42]. The underlying mechanism driving the emergence of such orientational order, however, remains elusive.

Here we analyze whether biological systems can exhibit this rather subtle phase by studying numerically and analytically the self-propelled Voronoi (SPV) model [13] of a tissue, including cell division and death. Our study demonstrates that the interaction between cell division and apoptosis and cell motility is key to initiating a hexatic phase. Without cell division, the model transitions from crystal to hexatic and then to liquid. Introducing cell division and motility, we observe complex liquid-hexatic and hexatic-liquid transitions, resulting in a reentrant phase diagram. This indicates that, contrary to traditional views, cell motility, in conjunction with cell division, promotes the hexatic state. We examine the role the relevant topological defects (dislocations and disclinations) play in establishing orientational order and develop a mean-field theory that accurately describes the emergence of hexatic order from the interplay of cell division and motility. This theory closely matches our simulations, with no fitting parameters,

and sheds light on the key mechanisms that lead to a hexatic phase.

Model.—We model a 2D cell layer using the SPV [13] version of the vertex model [40,43–48]. The cell shapes and the cellular network are determined based on the Voronoi tessellation [49,50] of the cell centers $\{\mathbf{r}_i\}$. Here mechanical interactions in the tissue are controlled by the energy functional $E = \sum_{i=1}^N [K_A(A_i - A_0)^2 + K_P(P_i - P_0)^2]$. The first term, quadratic in the cell areas $\{A_i\}$, originates from the incompressibility of cell volume, giving rise to a 2D area elasticity constant K_A and preferred area A_0 [43,51]. The second term, quadratic in the cell perimeters $\{P_i\}$, arises from the contractility of the cell cortex, with an elastic constant K_P [43]. Here P_0 is the target cell perimeter [12], representing the interfacial tension set by the competition between the cortical tension and the adhesion between adjacent cells [51]. The target shape index $p_0 = P_0/\sqrt{A_0}$ effectively characterizes the competition between cell-cell adhesion and cortical tension, acting as a signature for the solid-liquid phase transition [12,47]. Apart from the effective mechanical interaction force $\mathbf{F}_i = -\nabla_i E$, cells are self-propelled. A self-propulsion force is exerted along the cell polarity direction $\hat{\mathbf{n}}_i = (\cos \theta_i, \sin \theta_i)$, where θ_i is the polarity angle. The self-propulsion has a constant magnitude v_0/μ , with μ the inverse of a frictional drag. The equation of motion for each cell is given by

$$\dot{\mathbf{r}}_i = \mu \mathbf{F}_i + v_0 \hat{\mathbf{n}}_i. \quad (1)$$

The polarity angle obeys rotational diffusion: $d\theta_i/dt = \eta_i(t)$, where $\eta_i(t)$ is white noise [$\langle \eta_i(t) \eta_j(t') \rangle = 2D_r \delta(t - t') \delta_{ij}$], with D_r the rotational diffusion rate.

In addition to self-propulsion, cell division and apoptosis serve as additional sources of active force in living tissues [39,52–54]. Here, every cell has an equal division rate γ_0 . For each division, a daughter cell is introduced by randomly seeding a point at a distance of $d = 0.1$ (in units of the average cell diameter) near the mother cell [55]. In order to study the density-independent effects of cell division, we fix the number density of the tissue by implementing apoptosis at the same rate as division. Apoptosis is then performed on randomly chosen cells, removing cells from the tissue. This simulation scheme mimics the maintenance of homeostatic balance in a tissue [56–58].

The model is nondimensionalized by expressing all lengths in units of $\sqrt{\bar{A}}$, where \bar{A} is the average cell area, and time in units of $1/(\mu K_A \bar{A})$. Three independent parameters remain: the cell division and apoptosis rate γ_0 , the magnitude of motility v_0 , and the cell shape index p_0 . Throughout the simulations, we choose $D_r = 1$, without loss of generality. Tissue with N cells is simulated in a square box with size $\sqrt{N} \times \sqrt{N}$ under periodic boundary conditions. We numerically simulate the model using the open-source cellGPU [59]. The simulations start with a crystalline initial state in which cell centers form a

triangular lattice. Equation (1) is numerically integrated for 2×10^6 steps at step size $\Delta t = 0.05$. Here our analysis is based on the steady-state regime of the simulations (final 5×10^5 steps). In Supplemental Material Fig. S1 [60], we show that our results are the same for two distinct initial conditions (amorphous vs crystalline) as well as two different simulation protocols (heating vs cooling). Finally, we use $p_0 = 3.6$ in our simulations, except if otherwise stated.

Signature for the emergence of hexatic order.—Translational and orientational symmetries distinguish the three phases: crystalline, hexatic, and liquid. A 2D crystalline phase has quasi-long-range translational order and long-range orientational order, whereas the liquid phase has no long-range order of either kind. These two symmetries are related but not concomitant. The system in the hexatic phase has no long-range translational order but exhibits quasi-long-range orientational order [14,15]. Translational order at the cell level is measured by $\psi_T(\mathbf{r}_j) = \exp(i\mathbf{G}_r \cdot \mathbf{r}_j)$, where \mathbf{G}_r represents the reciprocal vector of the triangular lattice. The orientational order is measured by $\psi_6(\mathbf{r}_j) = (1/\sum_{i=1}^{z_j} l_{ij}) \sum_{i=1}^{z_j} l_{ij} \exp(i6\theta_i^j)$ [53,62–64], where the sum runs over the n neighbors of the cell and is weighted by their shared edge length [65]. θ_i^j is the angle of the neighboring joint vector $(\mathbf{r}_i - \mathbf{r}_j)$ to a reference axis. In Fig. 1, we plot the tissue-level order parameters, capturing only the magnitude, $\Psi_6 = |(1/N) \sum_{j=1}^N \psi_6(\mathbf{r}_j)|$ and $\Psi_T = |(1/N) \sum_{j=1}^N \psi_T(\mathbf{r}_j)|$ as a function of v_0 . In the absence of cell division (black lines), the tissue is a crystal at low v_0 where both Ψ_T

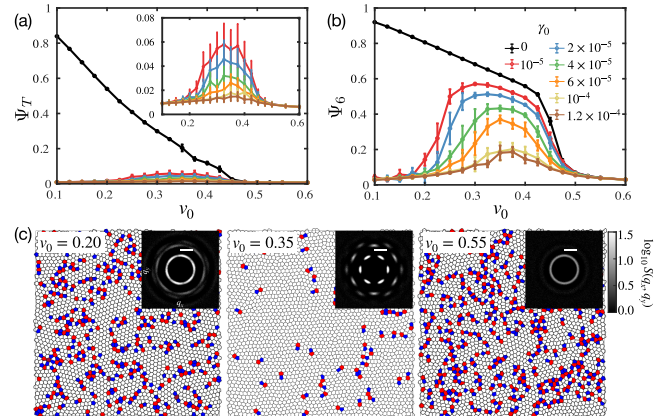


FIG. 1. (a) The translational order parameter Ψ_T and (b) the orientational order parameter Ψ_6 as a function of the cell motility v_0 at various division rates γ_0 . The error bar represents the standard deviation over the ensemble of random simulations. Inset of (a) shows a magnified view of (a). (c) Representative snapshots and the structure factor $S(\mathbf{q})$ for various v_0 at $\gamma_0 = 2 \times 10^{-5}$ corresponding to liquid, hexatic, and liquid states (from left to right). Colored cells correspond to disclinations of charge $q = +1$ (blue), -1 (red), and -2 (dark red). The state at $v_0 = 0.35$ is in the hexatic phase: it has dislocations, but no isolated disclinations.

and Ψ_6 are close to 1. The order parameters decrease monotonically with increasing v_0 . For $0.35 \lesssim v_0 \lesssim 0.45$, the tissue lacks translational order but retains orientational order, suggesting the existence of a hexatic phase before melting into a liquid phase at higher v_0 . This result is consistent with the ‘‘crystal-hexatic-liquid’’ melting scenario in a previous study using a similar model [33].

When cells divide [colored lines in Figs. 1(a) and 1(b)], Ψ_T is always close to zero for any value of v_0 . This clearly illustrates that activity due to cell cycling (division and death) always destroys the translational order and therefore forbids the formation of permanently frozen structures [39]. Remarkably, while an actively dividing tissue lacks translational order, it retains orientational order for a large range of v_0 values. This suggests the emergence of a hexatic phase at intermediate v_0 values. A transition from liquid to hexatic to liquid is visualized by the structure factor $S(\mathbf{q})$ for various v_0 at a fixed division rate [Fig. 1(c)].

To determine the location of the transitions between the phases, we next compute the spatial correlation functions, given by $g_\alpha(r) = \langle \psi_\alpha^*(r) \psi_\alpha(0) \rangle$, where $\alpha = 6, T$ corresponds to orientational and translational order, respectively. The peaks of correlations are fitted by a power-law decay $g_\alpha(r) \sim r^{-\eta_\alpha}$ (indicating quasi-long-range order) or an exponential decay $g_\alpha(r) \sim e^{-r/\xi_\alpha}$ (indicating short-range order).

The correlations are drawn and compared with the reference exponents from the Kosterlitz-Thouless-Halperin-Nelson-Young (KTHNY) theory [14,15,66–68] ($\eta_T = 1/3$ at the crystal-hexatic transition and $\eta_6 = 1/4$ at the hexatic-liquid transition) in Fig. 2 and Supplemental Material Fig. S2 [60]. Melting (without cell division) allows quasi-long-range translational order at low v_0 , decaying as a power law with $\eta_T \leq 1/3$. The translational order with cell division decays faster. Cell division also promotes the decay of bond-orientational correlations, but low γ_0 still allows for quasi-long-range $g_6(r)$ with $\eta_6 \leq 1/4$

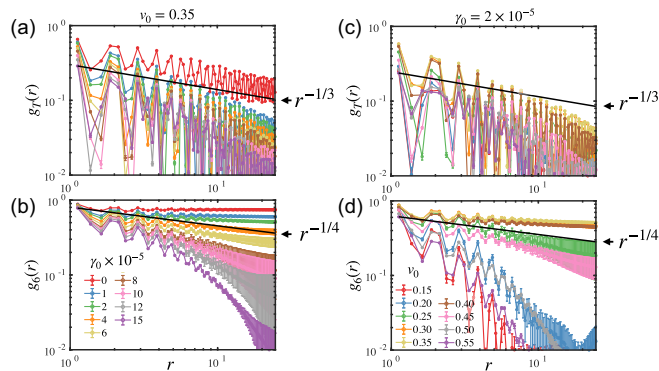


FIG. 2. The (a) translational and (b) orientational correlation functions at intermediate cell motility $v_0 = 0.35$ and varying γ_0 values. The (c) translational and (d) bond-orientational correlation functions at low cell division rate $\gamma_0 = 2 \times 10^{-5}$ and varying v_0 values.

at intermediate v_0 values. A broken translational symmetry without broken orientational symmetry characterizes the emergence of a hexatic state. Exponential decay fits the orientational order better in both low- and high- v_0 liquid phases.

The fitted exponents η_6 and ξ_6 at fixed division rate $\gamma_0 = 2 \times 10^{-5}$ and $\gamma_0 = 0$ (no division) are shown in Fig. 3 and in Supplemental Material Fig. S3 [60], respectively. These results confirm the emergence of two distinct liquid-hexatic and hexatic-liquid transitions when there is cell division. The correlations in the hexatic indeed display quasi-long-range order, well fitted by power-law decays, $g_6(r) \sim r^{-\eta_6}$, while outside the hexatic region correlations are short range and well fitted by exponential decays $g_6(r) \sim e^{-r/\xi_6}$. As the hexatic phase is approached from either side, ξ_6 grows rapidly, consistent with a diverging correlation length.

Despite excellent agreement with the KTHNY model, the correlation functions and the associated quantities (ξ_6, η_6) near the onset of the hexatic suffer from large sample-to-sample variations, as shown in Figs. 3(a) and 3(b). We have confirmed that this is not due to finite-size effects since, even at large system sizes, the behavior of $g_6(r)$ can range from exponential decay to a power-law decay (Supplemental Material Fig. S4 [60]). Consequently, (ξ_6, η_6) cannot be used to pinpoint the precise location of the liquid-hexatic and hexatic-liquid transitions. We therefore take advantage of the large fluctuations that arise near critical points by using the order parameter susceptibility to pinpoint the transitions. The susceptibility is given by $\chi_\alpha = N(\langle \Psi_\alpha^2 \rangle - \langle \Psi_\alpha \rangle^2)$, which characterizes the fluctuations in

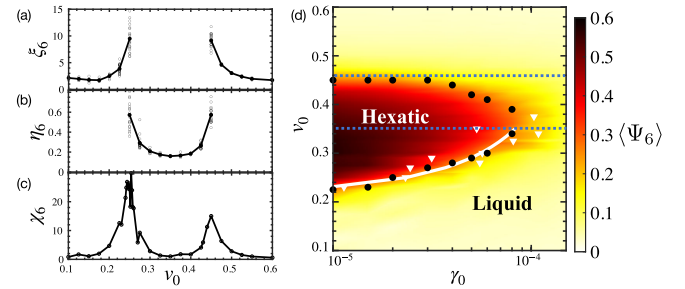


FIG. 3. (a) The orientational correlation length ξ_6 and (b) the power-law decay exponent η_6 of the orientational correlation function are shown as functions of v_0 at constant $\gamma_0 = 2 \times 10^{-5}$. The solid lines represent the mean values derived from the ensemble of simulations (indicated by circles). (c) The orientational susceptibility χ_6 vs v_0 at constant $\gamma_0 = 2 \times 10^{-5}$. (d) A phase diagram as a function of cell division rate γ_0 and motility v_0 . Here the color indicates the magnitude of the orientational order parameter. Black dots mark the peaks of χ_6 , which correspond to the hexatic-liquid transition. The blue dashed lines indicate the liquid-hexatic and hexatic-crystal transition points in the absence of cell division. The white triangles and solid line indicate when the rate of cell division balances the rate of cell-cell rearrangements, or $\langle \dot{Z} \rangle / 8 = \gamma_0$, where $\langle \dot{Z} \rangle$ is the intrinsic rate of cell-cell rearrangement attributed solely to motility.

the translational (χ_T) and orientational (χ_6) order parameters. Since χ_α is essentially an integral of the correlation function, it is expected to be more robust to finite-size or finite-time effects [20,31].

In the melting process without cell division (Supplemental Material Fig. S5 [60]), there is a sharp peak of χ_T at $v_0 = 0.35$, indicating a crystal-hexatic transition. On the other hand, χ_6 exhibits a sharp peak at $v_0 = 0.46 \pm 0.01$, corresponding to the hexatic-liquid transition. By analyzing system sizes ranging from $N = 2430$ to 38880, we show that the divergences of the susceptibilities are robust to finite-size effects [60].

In contrast, in the presence of cell division (i.e., a constant $\gamma_0 = 2 \times 10^{-5}$), χ_6 exhibits two clear peaks at $v_0 = 0.25 \pm 0.01$ and at $v_0 = 0.45 \pm 0.01$ [Fig. 3(c)]. Whereas the latter point is a vestige of the hexatic-liquid transition that occurs in the absence of cell division, the first transition point arises solely from the interplay of motility and cell division. Here, a state that would be crystalline in the absence of cell division becomes hexatic when cells divide. By analyzing susceptibilities to characterize the distinct phases, we systematically construct a phase diagram in the $v_0 - \gamma_0$ plane [Fig. 3(d)]. Here, for a fixed cell division rate, the tissue exhibits a reentrant transition from liquid to hexatic and back to liquid with increasing v_0 . Notably, the transition boundaries—both lower and upper—converge and eventually vanish for sufficiently high γ_0 . We also checked the p_0 dependence of the phase diagram in Supplemental Material Fig. S6 [60] and find qualitatively the same behavior as in [33], although the precise values of the transition line appear to be different.

Disclinations and dislocations.—According to the KTHNY theory [14,15,66–68], the distinct phases crystalline, hexatic, and liquid are characterized by the distributions of the basic topological defects known as disclinations and dislocations. Whereas the pure crystalline phase is defect-free—or, equivalently, all defects are tightly bound in defect-antidefect pairs—the hexatic phase has a nonvanishing density of free dislocations and the liquid phase has a nonvanishing density of free disclinations. We can define a charge $q_i = 6 - z_i$ [69] associated with disclinations, where z_i is the coordination number (number of neighbors) of the i th cell. Hexagonal cells are thus “neutral,” pentagonal cells have charge +1, heptagonal cells charge –1, and so on. Dislocations, the defects that disrupt translational order but preserve orientational order, correspond to tightly bound 5–7 pairs. They are neutral as disclinations, but possess a net vectorial charge, the Burgers vector. We approximate the Burgers vector by the displacement vector separating the five and the connected seven. In general, there will be clusters of connected defects and one must measure the associated disclination and dislocation charges of the entire cluster. The density of disclinations and dislocations are calculated by their volume fraction averaged over time. Representative

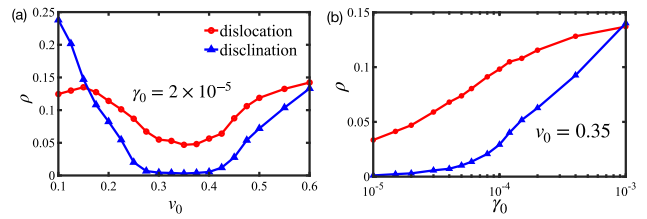


FIG. 4. (a) The volume densities of dislocations and disclinations are plotted as functions of v_0 at constant cell division rate $\gamma_0 = 2 \times 10^{-5}$. (b) The same quantities are plotted at a constant $v_0 = 0.35$ and varying γ_0 .

simulation snapshots in Fig. 1(c) and Supplemental Material Video S1 [60] show the evolution of dislocations and disclinations at various values of cell motility at a fixed division rate.

As shown in Fig. 4(a), cell division creates dislocations at a rate dependent on motility. Division tends to disorder, favoring a liquid. What about motility? At low motility, division disordering wins. At high motility, both processes generate disorder, leading again to a liquid. But for a significant range of intermediate motilities, we see that the number density of free disclinations falls to zero, whereas the free dislocation density is finite. How is this possible? In this intermediate region we hypothesize that disclinations are able to explore sufficient configuration space to access local free energy minima at which all disclinations find their antidisclinations and bind into dislocations, thus leading to a hexatic. Figure 4(b) further shows the defect-density dependence on cell division rate at a fixed motility in the hexatic regime, showing that sufficiently high division rates lead to a nonzero density of free disclinations, thus melting the hexatic to a liquid.

Taken together, it becomes evident that cell divisions not only introduce disclinations, but also that motility plays an essential role in generating cell-cell rearrangements that “heal” these defects, hence preserving orientational order. To analyze this within our simulations, we determine the intrinsic rate of cell-cell rearrangement attributed solely to motility by tracking how frequently a cell alters its neighbors, represented as \dot{Z} (see detailed method in Supplemental Material [60]). It is important to note that a cell can alter neighbors without undergoing uncaging, and, within the hexatic phase, it is this “rattling” behavior that serves as the primary means for stress relaxation, as opposed to α relaxation [70]. Remarkably, our findings indicate that when the rate of cell division (γ_0) surpasses the mean rate of neighbor changes ($\langle \dot{Z} \rangle$), there is a proliferation of disclination defects within the tissue, leading to a liquid state. Conversely, when the rate driven by γ_0 is less than $\langle \dot{Z} \rangle$, the tissue manifests global hexatic order. Figure 3(d) illustrates that the demarcation between liquid and hexatic states aligns precisely with the condition $\langle \dot{Z} \rangle / 8 = \gamma_0$ (details given in [60]).

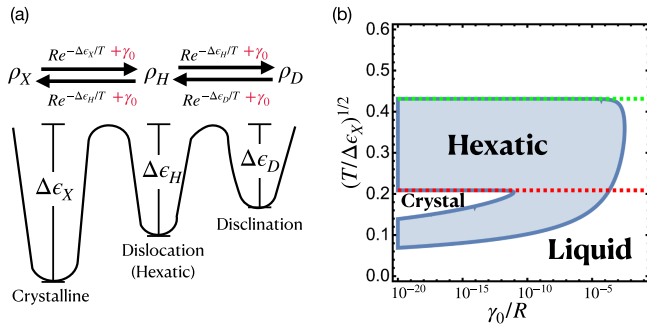


FIG. 5. A mean-field description for defect dynamics in a tissue. (a) The energy landscape and transition diagram between states. (b) The phase diagram of mean-field model as a function of the dimensionless division rate γ_0/R and motility $(T/\Delta\epsilon_X)^{1/2}$. The green (red) dashed line indicates the liquid-hexatic and hexatic-crystal transition in the absence of cell division.

Mean-field model.—Motivated by the dynamics of defects, we develop a simple mean-field (MF) model to better understand the emergence of hexatic order through cell division (Fig. 5). We simplify the state of a small cell cluster (~ 4 cells) using a mean-field approximation that allows three states: (a) crystalline solid state (“ordered”), (b) an isolated single dislocation, and (c) an isolated single disclination. Transitions between states arise from fluctuations over the energy barriers $\Delta\epsilon_i$, as illustrated in Fig. 5(a). Fluctuations arise from both Brownian motility forces and cell division, leading, in the low temperature limit, to an equal density distribution of states rather than only the ordered state [60]. In the steady-state limit [Fig. 5(b)], the asymmetric boundary of the hexatic region (determined by the threshold of ρ_H and ρ_D) is remarkably similar to our simulations and the phase diagram shows a reentrant liquid-hexatic-liquid transition with changing motility, as in Fig. 3(d). The MF model predicts a unique behavior for ultralow division rates ($\gamma_0/R \ll 10^{-10}$), where tissues undergo a complex temperature-dependent transition sequence, following a liquid-hexatic-crystal-hexatic-liquid path at constant γ_0/R [Fig. 5(b)]. As γ_0/R decreases further, the temperature range for the crystalline phase expands and ultimately converges with the crystalline phase present at $\gamma_0/R = 0$ (see [60] for a detailed discussion). The behavior at $(\gamma_0 = 0, T = 0)$ exhibits an interesting path dependence (i.e., taking the limit of $\gamma_0 \rightarrow 0$ while $T = 0$ vs taking the limit of $T \rightarrow 0$ while $\gamma_0 = 0$), as shown in Fig. S10 [60]. Remarkably, our phase diagram closely mirrors that of 2D melting on a random substrate [71]. In both models, temperature drives phase transitions, and in our case, cell division plays a role analogous to substrate disorder, introducing persistent, random spatial distortions.

Discussion.—The subtle balance required to establish hexatic order in equilibrium means that it is often confined to a rather narrow region of the relevant parameter space.

Our findings suggest that cell division provides a new way of exploring the configuration space of physical systems, as noted above. In particular, the dynamics of dislocation defects generated by cell division, both self-propelled and relaxational, promote fluctuations over barriers separating the hexatic phase from crystalline or liquid phases. This phenomenon, which we may call defect-driven structure development, may well have implications beyond biological systems. In terms of the configuration space explored by the vertex model, cell division and apoptosis correspond to adding $T2$ moves (interstitial insertion and deletion) to the allowed lattice updates—this yields a more efficient exploration of the space of all Voronoi tessellations and thus better routes to local hexatic minima [72–74]. It is remarkable that the early work of Swope and Andersen [75] found the hexatic phase by employing a grand canonical ensemble in which particles are added and removed. The mechanism we find here is very different from that found in colloids [20] and models of active particles [76], where packing density plays a crucial role.

Our Letter provides a clear framing of the essential criteria for hexatic order within proliferating tissues. We claim that hexatic order can be maintained when the rate of cell-cell rearrangements, induced by motility, surpasses the rate of cell division and apoptosis. This hypothesis presents a clear pathway for experimental validation and should be testable in both developing [53,77] and *in vitro* tissue models [10,11].

We have assumed isotropic cell division, but including oriented divisions could enhance hexatic order. Recent work [53] demonstrated that oriented divisions induce fourfold orientational order *in vivo* via active defect climb, where defects in the emerging lattice from cell divisions are corrected by further divisions along a global polarity axis. The impact of oriented divisions on hexatic order warrants future investigation.

This work was supported in part by NSF DMR-2046683 (Y. T. and D. B.), PHY-1748958 (D. B. and M. J. B.), the Center for Theoretical Biological Physics NSF PHY-2019745 (Y. T. and D. B.), Alfred P. Sloan Foundation (Y. T. and D. B.), the Human Frontier Science Program (Y. T. and D. B.), and NIH R35GM15049 (D. B.).

-
- [1] T. Lecuit, P.-F. Lenne, and E. Munro, *Annu. Rev. Cell Dev. Biol.* **27**, 157 (2011).
 - [2] P. A. Janmey and R. T. Miller, *J. Cell Sci.* **124**, 9 (2011).
 - [3] T. Mammoto and D. E. Ingber, *Development (Cambridge, U.K.)* **137**, 1407 (2010).
 - [4] R. M. Tenney and D. E. Discher, *Curr. Opin. Cell Biol.* **21**, 630 (2009).
 - [5] L. Atia, D. Bi, Y. Sharma, J. A. Mitchel, B. Gweon, S. A. Koehler, S. J. DeCamp, B. Lan, J. H. Kim, R. Hirsch, A. F. Pegoraro, K. H. Lee, J. R. Starr, D. A. Weitz, A. C. Martin,

- J.-A. Park, J. P. Butler, and J. J. Fredberg, *Nat. Phys.* **14**, 613 (2018).
- [6] J.-A. Park *et al.*, *Nat. Mater.* **14**, 1040 (2015).
- [7] A. Mongera, P. Rowghanian, H. J. Gustafson, E. Shelton, D. A. Kealhofer, E. K. Carn, F. Serwane, A. A. Lucio, J. Giammona, and O. Campàs, *Nature (London)* **561**, 401 (2018).
- [8] C. Malinverno *et al.*, *Nat. Mater.* **16**, 587 (2017).
- [9] T. E. Angelini, E. Hannezo, X. Trepát, M. Marquez, J. J. Fredberg, and D. A. Weitz, *Proc. Natl. Acad. Sci. U.S.A.* **108**, 4714 (2011).
- [10] S. Garcia, E. Hannezo, J. Elgeti, J.-F. Joanny, P. Silberzan, and N. S. Gov, *Proc. Natl. Acad. Sci. U.S.A.* **112**, 15314 (2015).
- [11] A. Puliafito, L. Hufnagel, P. Neveu, S. Streichan, A. Sigal, D. K. Fygenson, and B. I. Shraiman, *Proc. Natl. Acad. Sci. U.S.A.* **109**, 739 (2012).
- [12] D. Bi, J. H. Lopez, J. M. Schwarz, and M. L. Manning, *Nat. Phys.* **11**, 1074 (2015).
- [13] D. Bi, X. Yang, M. C. Marchetti, and M. L. Manning, *Phys. Rev. X* **6**, 021011 (2016).
- [14] B. I. Halperin and D. R. Nelson, *Phys. Rev. Lett.* **41**, 121 (1978).
- [15] D. R. Nelson and B. I. Halperin, *Phys. Rev. B* **19**, 2457 (1979).
- [16] C.-F. Chou, A. J. Jin, S. W. Hui, C. C. Huang, and J. T. Ho, *Science* **280**, 1424 (1998).
- [17] C. A. Murray, in *Bond-Orientational Order in Condensed Matter Systems*, Partially Ordered Systems, edited by K. J. Strandburg (Springer, New York, 1992), p. 137, [10.1007/978-1-4612-2812-7_4](https://doi.org/10.1007/978-1-4612-2812-7_4).
- [18] K. Zahn, R. Lenke, and G. Maret, *Phys. Rev. Lett.* **82**, 2721 (1999).
- [19] K. Zahn and G. Maret, *Phys. Rev. Lett.* **85**, 3656 (2000).
- [20] Y. Han, N. Y. Ha, A. M. Alsayed, and A. G. Yodh, *Phys. Rev. E* **77**, 041406 (2008).
- [21] R. Seshadri and R. M. Westervelt, *Phys. Rev. Lett.* **66**, 2774 (1991).
- [22] C. M. Knobler and R. C. Desai, *Annu. Rev. Phys. Chem.* **43**, 207 (1992).
- [23] C. C. Huang, in *Bond-Orientational Order in Condensed Matter Systems*, Partially Ordered Systems, edited by K. J. Strandburg (Springer, New York, 1992), pp. 78–136.
- [24] C. Huang and T. Stoebe, *Adv. Phys.* **42**, 343 (1993).
- [25] R. Podgornik, H. H. Strey, K. Gawrisch, D. C. Rau, A. Rupperecht, and V. A. Parsegian, *Proc. Natl. Acad. Sci. U.S.A.* **93**, 4261 (1996).
- [26] D. H. Van Winkle, A. Chatterjee, R. Link, and R. L. Rill, *Phys. Rev. E* **55**, 4354 (1997).
- [27] R. L. Rill, T. E. Strzelecka, M. W. Davidson, and D. H. Van Winkle, *Physica (Amsterdam)* **176A**, 87 (1991).
- [28] D. J. Bishop, P. L. Gammel, and C. A. Murray, in *The Vortex State*, NATO ASI Series, edited by N. Bontemps, Y. Bruynseraede, G. Deutscher, and A. Kapitulnik (Springer Netherlands, Dordrecht, 1994), pp. 99–123.
- [29] C. A. Murray, P. L. Gammel, D. J. Bishop, D. B. Mitzi, and A. Kapitulnik, *Phys. Rev. Lett.* **64**, 2312 (1990).
- [30] Y.-W. Li and M. P. Ciamarra, *Phys. Rev. Mater.* **2**, 045602 (2018).
- [31] M. Durand and J. Heu, *Phys. Rev. Lett.* **123**, 188001 (2019).
- [32] R. xue Guo, J. Jian Li, and B. quan Ai, *Physica (Amsterdam)* **623A**, 128833 (2023).
- [33] A. Pasupalak, L. Yan-Wei, R. Ni, and M. P. Ciamarra, *Soft Matter* **16**, 3914 (2020).
- [34] B. Loewe, M. Chiang, D. Marenduzzo, and M. C. Marchetti, *Phys. Rev. Lett.* **125**, 038003 (2020).
- [35] M. Paoluzzi, L. Angelani, G. Gosti, M. C. Marchetti, I. Pagonabarraga, and G. Ruocco, *Phys. Rev. E* **104**, 044606 (2021).
- [36] J. jian Li and B. quan Ai, *New J. Phys.* **23**, 083044 (2021).
- [37] R. Cohen, L. Amir-Zilberstein, M. Hersch, S. Woland, O. Loza, S. Taiber, F. Matsuzaki, S. Bergmann, K. B. Avraham, and D. Sprinzak, *Nat. Commun.* **11**, 5137 (2020).
- [38] S. Hilgenfeldt, S. Eriskén, and R. W. Carthew, *Proc. Natl. Acad. Sci. U.S.A.* **105**, 907 (2008).
- [39] D. A. Matoz-Fernandez, K. Martens, R. Sknepnek, J. L. Barrat, and S. Henkes, *Soft Matter* **13**, 3205 (2017).
- [40] J. A. Mitchel, A. Das, M. J. O’Sullivan, I. T. Stancil, S. J. DeCamp, S. Koehler, O. H. Ocaña, J. P. Butler, J. J. Fredberg, M. A. Nieto, D. Bi, and J.-A. Park, *Nat. Commun.* **11**, 5053 (2020).
- [41] T. Kanasaki, C. M. Edwards, U. S. Schwarz, and J. Grosshans, *Integr. Biol.* **3**, 1112 (2011).
- [42] F. Kaiser, Z. Lv, D. Marques Rodrigues, J. Rosenbaum, T. Aspelmeier, J. Großhans, and K. Alim, *Biophys. J.* **114**, 1730 (2018).
- [43] R. Farhadifar, J.-C. Röper, B. Aigouy, S. Eaton, and F. Jülicher, *Curr. Biol.* **17**, 2095 (2007).
- [44] X. Li, A. Das, and D. Bi, *Phys. Rev. Lett.* **123**, 058101 (2019).
- [45] X. Li, A. Das, and D. Bi, *Proc. Natl. Acad. Sci. U.S.A.* **115**, 6650 (2018).
- [46] S.-Z. Lin, D. Bi, B. Li, and X.-Q. Feng, *J. R. Soc. Interface* **16**, 20190258 (2019).
- [47] L. Yan and D. Bi, *Phys. Rev. X* **9**, 011029 (2019).
- [48] A. Das, S. Sastry, and D. Bi, *Phys. Rev. X* **11**, 041037 (2021).
- [49] G. L. Dirichlet, *J. Reine Angew. Math.* **1850**, 209 (1850).
- [50] H. Honda, *J. Theor. Biol.* **72**, 523 (1978).
- [51] D. B. Staple, R. Farhadifar, J. C. Röper, B. Aigouy, S. Eaton, and F. Jülicher, *Eur. Phys. J. E* **33**, 117 (2010).
- [52] A. Doostmohammadi, S. P. Thampi, T. B. Saw, C. T. Lim, B. Ladoux, and J. M. Yeomans, *Soft Matter* **11**, 7328 (2015).
- [53] D. J. Cislo, F. Yang, H. Qin, A. Pavlopoulos, M. J. Bowick, and S. J. Streichan, *Nat. Phys.* **19**, 1201 (2023).
- [54] T. B. Saw, A. Doostmohammadi, V. Nier, L. Kocgozlu, S. Thampi, Y. Toyama, P. Marcq, C. T. Lim, J. M. Yeomans, and B. Ladoux, *Nature (London)* **544**, 212 (2017).
- [55] We have checked that the results are independent of the choice of d .
- [56] M. Basan, J. Prost, J.-F. Joanny, and J. Elgeti, *Phys. Biol.* **8**, 026014 (2011).
- [57] J. Ranft, M. Basan, J. Elgeti, J.-F. Joanny, J. Prost, and F. Jülicher, *Proc. Natl. Acad. Sci. U.S.A.* **107**, 20863 (2010).
- [58] M. Czajkowski, D. M. Sussman, M. Cristina Marchetti, and M. Lisa Manning, *Soft Matter* **15**, 9133 (2019).
- [59] D. M. Sussman, *Comput. Phys. Commun.* **219**, 400 (2017).

- [60] See Supplemental Material at <http://link.aps.org/supplemental/10.1103/PhysRevLett.132.218402>, which includes Ref. [61], for additional details about methods, mean-field theory, and additional results complementing those shown in the main text.
- [61] D. Bi, J. H. Lopez, J. M. Schwarz, and M. L. Manning, *Soft Matter* **10**, 1885 (2014).
- [62] W. Mickel, S. C. Kapfer, G. E. Schröder-Turk, and K. Mecke, *J. Chem. Phys.* **138**, 044501 (2013).
- [63] J.-M. Armengol-Collado, L. N. Carenza, and L. Giomi, *eLife* **13**, e86400 (2024).
- [64] J.-M. Armengol-Collado, L. N. Carenza, J. Eckert, D. Krommydas, and L. Giomi, *Nat. Phys.* **19**, 1773 (2023).
- [65] Following [53,63,64], we weight cellular neighbors by their edge lengths, minimizing the influence of shorter edges. Our simulations indicate that short edges are rare, and employing the traditional, unweighted Ψ_6 definition yields comparable results, suggesting minimal impact of edge length on our findings.
- [66] A. P. Young, *Phys. Rev. B* **19**, 1855 (1979).
- [67] J. M. Kosterlitz and D. J. Thouless, *J. Phys. C* **6**, 1181 (1973).
- [68] E. P. Bernard and W. Krauth, *Phys. Rev. Lett.* **107**, 155704 (2011).
- [69] M. J. Bowick and L. Giomi, *Adv. Phys.* **58**, 449 (2009).
- [70] L. Berthier and G. Biroli, *Rev. Mod. Phys.* **83**, 587 (2011).
- [71] S. Sachdev and D. R. Nelson, *J. Phys. C* **17**, 5473 (1984).
- [72] M. Bowick, H. Shin, and A. Travasset, *Phys. Rev. E* **75**, 021404 (2007).
- [73] W. T. M. Irvine, M. J. Bowick, and P. M. Chaikin, *Nat. Mater.* **11**, 948 (2012).
- [74] M. J. Bowick, D. R. Nelson, and H. Shin, *Phys. Chem. Chem. Phys.* **9**, 6304 (2007).
- [75] W. C. Swope and H. C. Andersen, *J. Chem. Phys.* **102**, 2851 (1995).
- [76] P. Digregorio, D. Levis, A. Suma, L. F. Cugliandolo, G. Gonnella, and I. Pagonabarraga, *Phys. Rev. Lett.* **121**, 098003 (2018).
- [77] X. Wang, M. Merkel, L. B. Sutter, G. Erdemci-Tandogan, M. L. Manning, and K. E. Kasza, *Proc. Natl. Acad. Sci. U.S.A.* **117**, 13541 (2020).